Korean J. Chem. Eng., 39(1), 96-108 (2022)
DOI: 10.1007/s11814-021-0844-y

pISSN: 0256-1115
eISSN: 1975-7220

Enhanced adsorptive-oxidative desulfurization of dibenzothiophene over Ti-MWW using cumene hydroperoxide as oxidant

Xingye Zeng*, Adeyemo Adesina*, Ping Li, Hanlu Wang*,†, and Rujin Zhou*,†**

*Key Laboratory of Inferior Crude Oil Processing of Guangdong Provincial Higher Education Institutes, Guangdong University of Petrochemical Technology, Maoming, 525000, P. R. China
**Production Management Department, Sinopec Maoming Petrochemical Company, Maoming, 525000, P. R. China
(*Received 4 February 2021 • Revised 7 May 2021 • Accepted 12 May 2021*)

Abstract−Ti-containing Mobil composition of matter-twenty-two (Ti-MWW) zeolite was prepared via a two-step post-synthesis process and then characterized by X-ray fluorescence, nitrogen adsorption-desorption isotherms, Fourier transform infrared absorption spectra, X-ray diffraction, scanning electron microscopy, transmission electron microscopy, and X-ray photoelectron spectra. These results indicate that the textural properties of MWW were well preserved after acid treatment and incorporation of titanium. An adsorptive-oxidative desulfurization (AODS) system was successfully developed on the basis of a model oil containing dibenzothiophene (DBT) with the as-prepared Ti-MWW being the catalyst and adsorbent and cumene hydroperoxide (CHP) being the oxidant. The parameters influencing the desulfurization performance were systematically investigated. These parameters include the Ti-MWW dosage, the reaction temperature, the stirring speed, the molar ratio of CHP to DBT and the additions of olefins and aromatics to the system. The conversion rate of DBT reached 99.6% via the catalytic oxidation process and the turnover frequency was 40.1 h^{-1}. Meanwhile, the oxidation products of DBT were removed by Ti-MWW adsorption. The recycling and regeneration performance of Ti-MWW were also investigated, and the DBT conversion reached 99.5% using the regenerated Ti-MWW. This work provides useful information for the construction of solvent-free oxidative desulfurization systems using a zeolite.

Keywords: Adsorptive-oxidative Desulfurization, Ti-MWW, Dibenzothiophene, Cumene Hydroperoxide

INTRODUCTION

Fuel oils contain various heterocyclic sulfur-containing compounds (HSCs), such as benzothiophene, dibenzothiophene (DBT), and their alkyl substituted derivatives, which are difficult to remove efficiently by conventional hydrodesulfurization (HDS) [1]. However, faced with increasingly strict environmental regulations, it is imperative to develop alternative or supplementary desulfurization technologies for the production of low sulfur-content fuel oils [2]. Given the inherent difficulties of HDS, development of various non-HDS technologies is being introduced, such as extractive desulfurization [3], membrane separation desulfurization [4], photocatalytic desulfurization [5], adsorptive desulfurization [6], and oxidative desulfurization (ODS) [7]. These desulfurization processes can be operated under milder conditions and exhibit effective removal performance for HSCs.

Among the aforementioned processes, ODS has been reported to be more promising and effective since it can be applied at mild temperatures and pressures with no hydrogen consumption. The basic idea of ODS is to oxidize sulfur-containing compounds to highly polar compounds and then remove them by extraction or adsorption. A variety of extractants have been used in ODS systems, such as acetonitrile [8], dimethyl-formamide [9] and methanol [10]. However, these solvents are still slightly miscible with fuel oil [11]. As a result, this will bring additional pollution into the fuel during the desulfurization process to reduce oil quality. More seriously, these undesirable pollutant compounds usually contain nitrogen compounds which also strictly limit the ability to achieve cleaner fuel oils [12].

To avoid contamination of the treated oil by the extractant, another approach is to combine the adsorption with the ODS process under solvent-free conditions. This approach is commonly referred to as adsorptive-oxidative desulfurization (AODS). In the AODS process, the oxidized sulfur-containing compounds are adsorbed by the adsorbent, which is the additional adsorbent produced after the oxidation reaction or could be the catalyst itself. Then the clean oil is obtained by a solid-liquid separation, which reduces the additional pollution of the oil phase. From the perspective of solvent savings and green chemical usage, AODS is a promising approach for the production of clean oils.

Achieving efficient oxidation of sulfur-containing compounds is a critical step in an AODS process. Consequently, the choice of the oxidant should be considered first. Hydrogen peroxide (H_2O_2) is often chosen because of its single oxidation product [13]. However, H_2O_2 in most ODS systems is utilized as the oxidant which is immiscible with the oil, so the inter-solubility of H_2O_2 and DBT is not satisfactory [14]. Therefore, many attempts have been made to introduce oil-soluble oxidants into ODS and some examples include *t*-butyl hydroperoxide (TBHP) [15-17], cyclohexanone peroxide (CYHPO) [18,19], and cumene hydroperoxide (CHP) [20]. Among

†To whom correspondence should be addressed.
E-mail: wanghlu@mail2.sysu.edu.cn, rujinzhou@126.com

them, CHP as a commodity chemical and intermediate of phenol production, is cheap and commercially available. Moreover, its reductive product, 2-phenyl-2-propanol (cumyl alcohol, CA), can be directly used as an oil composition with a high value of octane number, or at least will not decrease the oil quality [21]. Herein, CHP was utilized as a preferred oxidant rather than H_2O_2.

The catalyst employed is another important factor affecting desulfurization efficiency. Mobil composition of matter-twenty-two (MWW) zeolite, consists of 12-membered ring side cups, two independent interlayer and 10-membered ring channels, one of which contains super cages of 0.71 nm×1.8 nm in dimension [22]. Therefore, the MWW framework zeolite can provide enough open reaction space to handle huge reactants in the super cage and side cups. This unique and unusual crystalline structure can be a good choice for adsorbing the oxidized sulfur-containing compounds [23]. However, the MWW framework has few active sites and it is difficult to achieve a satisfactory catalytic effect on its own [24]. One feasible method for improvement is to load some acidic catalytic active sites to the MWW framework. For instance, our group previously reported a catalyst, phosphotungstic acid supported by MWW, which showed a high catalytic activity for oxidative desulfurization [25]. However, the supported active sites were found to be easy to be lost during the reactions of interest in that study. Another method is to introduce variable valence metals, such as titanium (Ti) [26], into the molecular framework to construct catalytic active sites. Ti-MWW is a Ti-containing zeolite formed by introducing titanium into MWW framework. It not only has the catalytic oxidation of Ti, but also the shape selectivity and excellent stability of MWW. Because of its excellent oxidation and selectivity, Ti-MWW has been widely used in many specific oxidation reactions, such as limonene oxidation [27] and phenol hydroxylation [28]. Furthermore, it is also theoretically revealed that Ti-MWW is a potential catalyst for DBT oxidation reactions as detailed in a previous report [29]. Recently, Ti-containing zeolites have attracted much attention in the ODS reaction, like TS-1 [30,31], Ti-modified hierarchical mordenites [32], Ti-MCM-41 [33], Ti-HMS [34], and Ti-SBA-2 [35], which exhibited good catalytic oxidative performance for HSCs. These inspiring reports prompted us to further explore Ti-MWW for the desulfurization of fuel oils. However, there is still a lack of exploration for AODS composed of Ti-MWW and CHP.

The aim of this work is to investigate the DBT catalytic oxidation and adsorptive removal over Ti-MWW using CHP as the oxidant. A series of Ti-MWW with different Ti content were synthesized by a two-step post synthesis process, which included dealumination by acid treatment and incorporation of Ti by calcination with titanocene dichloride (Cp_2TiCl_2). The catalytic performance of the as-prepared Ti-MWW was evaluated mainly by the conversion of DBT in the AODS reaction. The parameters that influence the desulfurization performance were systematically investigated and these parameters included the Ti-MWW dosage, the reaction temperature (T), the stirring speed (v), the molar ratio of CHP to DBT (O/S), and the addition of olefins and aromatics to the system. Catalyst recycling and regeneration were also investigated.

EXPERIMENTAL

1. Materials

All the chemicals except CHP were of analytical grade and used as received without further purification. DBT (99 wt%), 1-octene (98 wt%), 1,2,3,4-tetrahydronaphthalene (98 wt%), 1,5-cyclo-octadiene (99 wt%), naphthalene (99 wt%), Cp_2TiCl_2 (97 wt%), decane (98 wt%), tetradecane (99 wt%), and CHP (80 wt% in cumene) were purchased from Aladdin Industrial Corporation (Shanghai, China). MWW was obtained from Shenyu Environmental Protection New Material Co., Ltd (China). Other chemical reagents were purchased from Tianjin Kernel Chemical Reagent Co., Ltd (China).

2. Synthesis of the Ti-MWW

Ti-MWW was prepared through a two-step post-synthesis procedure according to a method detailed in a previous report on the synthesis of Ti-Beta [36]. First, 5 g of commercial MWW (CM-MWW) was soaked in 50 mL of concentrated nitric acid (~68 wt%) for 20 h. The wet mixture was washed with deionized water until the pH value of the filtrate became neutral. After drying at 80 °C overnight, the acid treated MWW (AT-MWW) powder obtained was ground. Then, four different Ti-MWW were prepared, and the ratios of AT-MWW and Cp_2TiCl_2 are listed in Table 1. Specifically, the AT-MWW was completely ground with Cp_2TiCl_2 to obtain an intimate mixture of the two solids. The AT-MWW-Cp_2TiCl_2 mixtures were then calcinated in flowing air at 550 °C for 12 h to derive Ti-MWW. After cooling and grinding, the target product was obtained. The prepared Ti-MWW samples were denoted as Ti-MWW-1, Ti-MWW-2, Ti-MWW-3, and Ti-MWW-4, respectively, corresponding to the expected Ti loadings of 2.5, 5, 7.5, and 10 wt%.

3. Characterization of the Samples

The contents of Si, Al, and Ti were measured using a semi-quantitatively X-ray fluorescence (XRF) analysis on an AXIOS (Panako) XRF spectrometer. The X-ray diffraction (XRD) patterns of the prepared samples were recorded on a Rigaku Ultima IV instrument. Fourier transform infrared (FT-IR) spectra of the prepared samples in KBr pellets were carried out on Nicolet 380 FT-IR spectrometer over the range of 4,000-400 cm^{-1}. Scanning electron microscope (SEM) images were obtained using a Fei Inspect F50 field emis-

Table 1. Ratio of raw materials for preparing Ti-MWW

Sample	AT-MWW/g	Cp_2TiCl_2/g	Expected Ti loadings/wt%
Ti-MWW-1	0.99	0.131	2.5
Ti-MWW-2	0.95	0.262	5.0
Ti-MWW-3	0.925	0.393	7.5
Ti-MWW-4	0.90	0.524	10

Table 2. Physicochemical properties of the samples

Sample	Si/Al	Ti loadings/wt%	Si/Ti	$S_{BET}/(m^2 \cdot g^{-1})$	$V_{total}/(cm^3 \cdot g^{-1})$	$V_{micro}/(cm^3 \cdot g^{-1})$	$V_{meso}/(cm^3 \cdot g^{-1})$
CM-MWW	10.79	0.013	2,457	353.7	0.438	0.112	0.332
AT-MWW	12.83	0.020	2,428	349.3	0.437	0.117	0.329
Ti-MWW-1	12.62	2.92	24	324.0	0.402	0.116	0.292
Ti-MWW-2	12.53	5.82	12	318.6	0.327	0.100	0.232
Ti-MWW-3	12.72	8.44	8	309.9	0.293	0.100	0.198
Ti-MWW-4	12.20	11.10	5	301.6	0.326	0.092	0.247

sion scanning electron microscope. The energy dispersive X-ray spectroscopy (EDS) analysis was collected on an Oxford energy spectrometer. Transmission electron microscope (TEM) images were obtained using the TEM machine Fei Technai G20 F20. X-ray photoelectron spectra (XPS) were recorded on an Escalab 250xi photoelectron spectrometer with a mono-chromate Al-Kα X-ray source (hν=1,486.6 eV). The C 1s peak at 284.8 eV was used as the reference for determining the binding energies. The XPS peaks was deconvoluted based on PeakFit v4.12 program using the Gaussian fitting method. The N_2 isotherms of the samples collected under the constant temperature of liquid nitrogen using a Jingwei Gaobao JW-BK100 analyzer. Before the measurements, the samples were degassed at 150 °C for 4 h under vacuum to ensure a clean surface. The Brunauer-Emmett-Teller (BET) surface areas (S_{BET}) were determined from the N_2 adsorption at relative pressures of $0.05<P/P_0<0.3$. The total pore volume (V_{total}) was evaluated by a single-point method at a relative N_2 pressure of 0.95. The micropore volume (V_{micro}) was estimated using the *t*-plot, while the mesopore pore volume (V_{meso}) was expressed as a Barrett-Joyner-Halenda (BJH) adsorption cumulative total pore volume (pore diameter 1.7-300 nm).

4. DBT Conversion Test

The model oil containing DBT was prepared with a sulfur content of 500 $mg \cdot L^{-1}$ as follows. 1.4395 g of DBT was dissolved in 80 mL of *n*-decane and 10 mL of *n*-tetradecane. N-tetradecane was used as an internal standard to quantify the content of DBT. This solution was then transferred to a 500 mL volumetric flask and *n*-decane was added to make up the mixture to the scale line.

The DBT conversion test was performed in a 50 mL double jacketed glass flask equipped with a cryogenic liquid condenser under atmospheric pressure. The catalyst and CHP were preferentially added to the reaction flask and then 10 mL of the model oil was added. The mixture was preheated at a constant temperature of 30 °C for 5 min to exclude the effects of room temperature fluctuations. Then, the constant temperature water that reached the preset reaction temperature was quickly introduced into the jacket of the reactor and the reaction time was recorded. A magnetic stirrer with an adjustable speed was used to control the stirring rate at a constant speed that ranged from 250-750 rpm depending on the condition chosen for the run. 50 μL of the oil samples were collected and centrifuged periodically. The DBT concentration in the oil phase was determined using gas chromatography with flame ionization detection on an Agilent GC 7890B (HP-5 column, *l* 30 m×Φ 0.32 mm×0.25 μm). The conversion rate of DBT (η) was calculated based on Eq. (1):

$$\eta = \left(1 - \frac{C_t}{C_0}\right) \times 100\% \quad (1)$$

where C_t (mg/L) is the DBT concentration at the reaction time of t min, and C_0 is the initial DBT concentration. For simplicity, the desulfurization rate of the entire AODS system can refer to the conversion rate of DBT, because almost all of the DBT can be removed after conversion.

RESULTS AND DISCUSSION

1. Textural Properties

XRF was applied to investigate the contents of Si, Al, and Ti for the samples examined in this report and these results are shown in Table 2. These results show that the contents of Ti in CM-MWW and AT-MWW were 0.013 wt% and 0.020 wt%, respectively. This may be due to introducing trace amounts of Ti during the preparation of CM-MWW. When CM-MWW was acidified, the molar ratio of Si to Al (Si/Al) increased reasonably from 10.79 to 12.83 due to a small amount of the loss of some Al atoms. After AT-MWW calcination with a corresponding amount of Cp_2TiCl_2, the actual Ti contents were 2.92, 5.82, 8.44, and 11.10 wt%, slightly higher than the expected values of 2.5, 5.0, 7.5, and 10 wt%, respectively. This was due to the small amount of residual template agent removed during the calcination process, resulting in a slightly higher

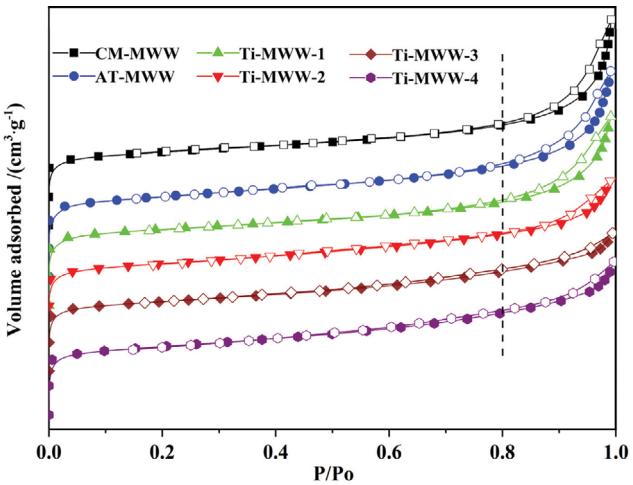

Fig. 1. N_2 adsorption/desorption isotherms for the samples (Solid legend: adsorption isotherm; Hollow legend: desorption: desorption isotherm).

Ti content.

The N_2 adsorption-desorption isotherms of the prepared samples are shown in Fig. 1. All of the isotherms exhibited a Type I isotherm according to the IUPAC classification, indicating that the samples belong to microporous materials [37]. When the relative pressure (P/P_0) was greater than 0.8, it was observed that all of the isotherms have obvious hysteresis loops (hysteresis type IV), which is attributed to the presence of mesopores between the aggregated crystals [38]. As the Ti content was gradually increased, the S_{BET}, V_{total}, and V_{mirco} were regularly reduced (Table 2). This is because the diameter and weight of the Ti atoms are larger than the Si atoms, which is the main cause of the decrease in the S_{BET} and V_{total} [39]. Notably, The V_{total} and V_{meso} of Ti-MWW-3 and Ti-MWW-4 showed opposite trends, because Ti is not fully integrated into the MWW framework in the case of high Ti content. Subsequent XPS characterization confirmed the existence of six-coordinated Ti-containing species (TiO_6) [40], which are different from the four-coordinated framework Ti. As shown in Fig. S1 in the supporting information (SI), the slight increase of V_{total} and V_{meso} is attributed to the accumulation of TiO_6 particles outside the framework. The S_{BET} and V_{micro} are mainly determined by the pores of MWW, so they still show a trend of decreasing regularity. It also indicated that there is an optimal value of Si/Ti to achieve a balance between reactive sites and surface area. Moreover, the AT-MWW sample has a slightly higher V_{micro} than the CM-MWW sample due to the loss of a small amount of Al atoms after acid treatment. This agreed with the results of the Si/Al characterized by XRF. The above results showed that the textural properties of the samples were well preserved after acid treatment and incorporation of Ti.

Fig. 2 shows that the XRD patterns of the samples were recorded in the 2θ range of 5-45°. All of the samples exhibited well-resolved diffraction peaks at 2θ=7.1, 8.0, 9.9, 14.3, 20.3, 22.7, 25.1, and 26.0°, correlated to the typical MWW type reflections of (100), (101), (102), (004), (212), (302), (220), and (310), respectively [41]. This indicates that the structure of the prepared samples can be well preserved after post-treatment and incorporation of Ti. Uniform narrow peaks extended to 2θ=26.0°, where diffraction peaks with decreasing intensity corresponded with the increase in the Ti loading during calcination. This implies that the (310) facet was most affected by the Ti content. No diffraction peak assigned to crystalline TiO_2 was observed, suggesting that no bulky TiO_2 was formed after incorporation of Ti [42]. However, this is not in contradiction with the above results inferred from N_2 adsorption-desorption isotherms, because these Ti-containing species outside the framework may be amorphous and difficult to detect by XRD.

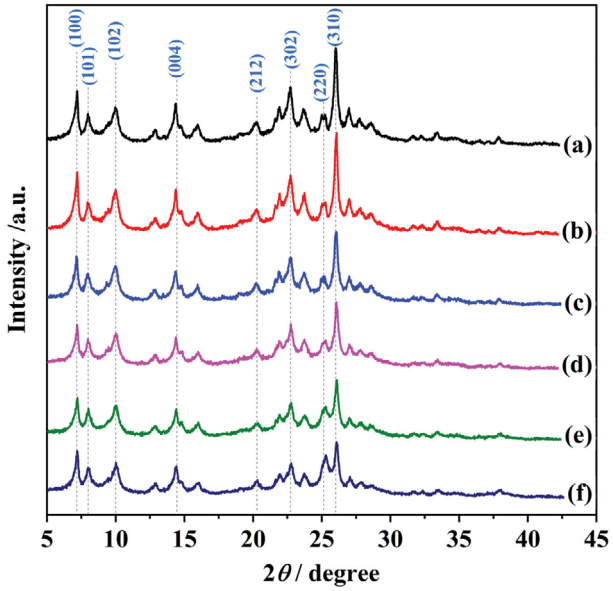

Fig. 2. XRD patterns of the samples: (a) CM-MWW, (b) AT-MWW, (c) Ti-MWW-1, (d) Ti-MWW-2, (e) Ti-MWW-3, and (f) Ti-MWW-4.

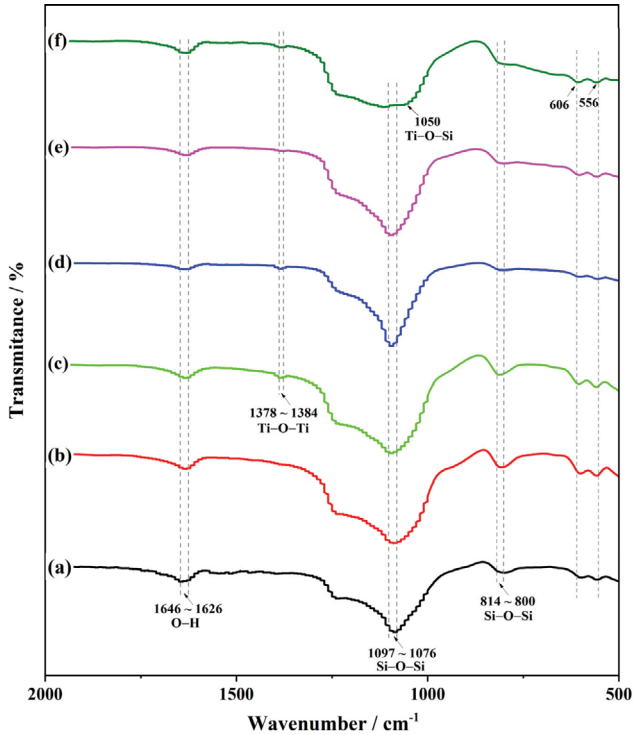

Fig. 3. FT-IR spectra of the samples: (a) CM-MWW, (b) AT-MWW, (c) Ti-MWW-1, (d) Ti-MWW-2, (e) Ti-MWW-3, and (f) Ti-MWW-4.

Fig. 3 depicts the FT-IR spectra in the framework vibrational frequency region (2,000-500 cm^{-1}) of the samples. The peaks at 556 and 606 cm^{-1} are characteristic of the framework vibrations of the MWW structure [37]. The peaks at 814-800 cm^{-1} correspond to the symmetric stretching of Si-O-Si, 1,097-1,076 cm^{-1} to the asymmetric Si-O-Si vibration, and 1,646-1,626 cm^{-1} to the bending vibration of the O-H groups [43]. The peaks at 1,646-1,626 cm^{-1} were observed for the bending vibration of the O-H groups. This is because part of the Al atoms are removed during the acid treatment, and then O-H groups are formed [44]. After the introduction of Cp_2TiCl_2 subsequently followed by calcination, a clear new peak at 1,378-1,384 cm^{-1} appeared in the samples of Ti-MWW-1, -2, -3, and -4, which belong to the stretching vibration of Ti-O-Ti. However, the peak at 1,050 cm^{-1} was observed on Ti-MWW-4, which belonged to the stretching vibration of Ti-O-Si. This can also be attributed to the successful incorporation of Ti atoms into the

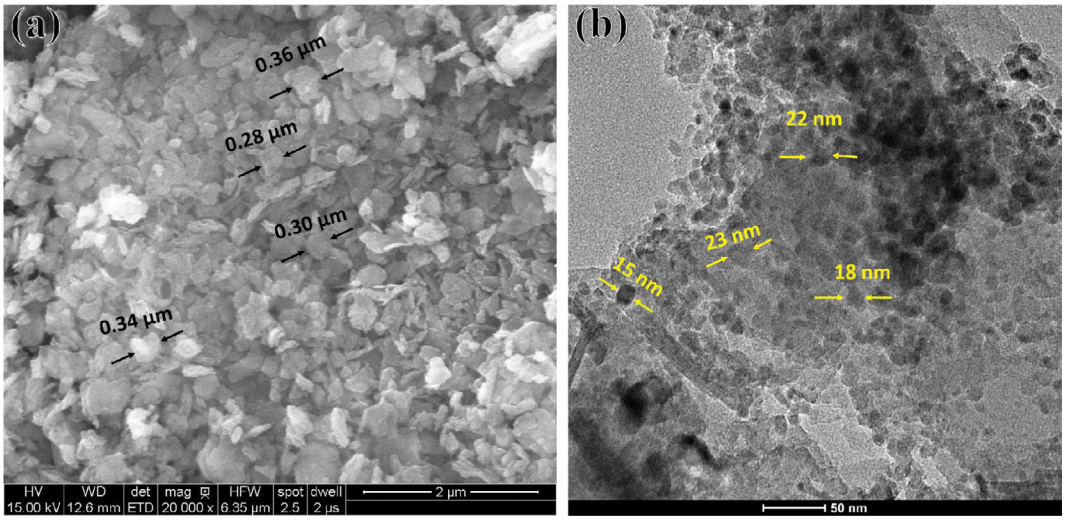

Fig. 4. (a) SEM and (b) TEM images of the Ti-MWW-4 sample.

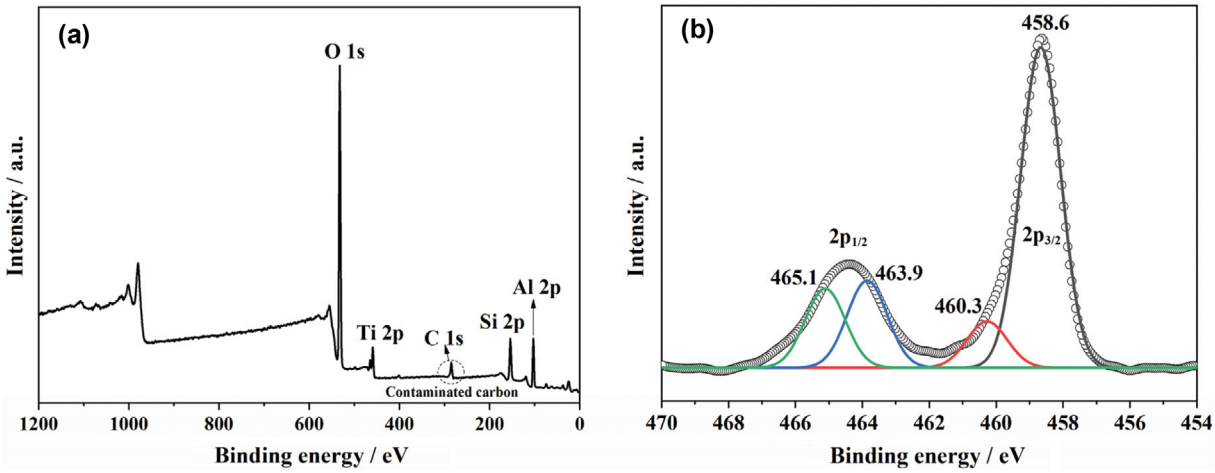

Fig. 5. XPS spectra of the Ti-MWW-4 sample: (a) survey and (b) Ti 2p.

framework. When the Ti content was low (<10 wt%), the stretching vibration of Ti-O-Si was not observed, probably due to some overlapping by the asymmetric Si-O-Si vibrational band.

Ti-MWW-4 was employed to further characterize the morphology of the sample. The SEM images of the Ti-MWW-4 exhibited that the particles are composed of disordered sheets agglomerated into 0.2 to 0.4 μm clusters (Fig. 4(a)). No other striking morphology was observed, which was consistent with the previous reports for Ti-MWW [27]. The TEM (Fig. 4(b)) results further reveal that the clusters are composed of rectangular or disk-shaped nanosheets with sizes in the range of 15 to 30 nm.

To validate the Ti coordination form of the as-synthesized Ti-MWW, the Ti-MWW-4 was further studied by XPS analysis as shown in Fig. 5. The XPS survey spectrum (Fig. 5(a)) revealed that the Ti-MWW-4 sample is mainly composed of Si, O, Al, and Ti elements. As shown in Fig. 5(b), the binding energy values of 460.3 eV and 465.1 eV can be ascribed to Ti $2p_{3/2}$ and Ti $2p_{1/2}$ photoelectrons of a tetrahedrally coordinated framework Ti species [45]. In addition, another group of peaks at 458.6 eV and 463.9 eV was also observed, indicating the presence of non-framework Ti species (TiO_6). This is due to the insufficient framework sites to accommodate Ti with the increase of Ti content, which leads to the formation of some non-framework Ti-containing species. Previous studies have shown that the activity of TiO_6 is 2-3 times higher than that of tetrahedral coordinated Ti [40]. This is also a key reason for the high desulfurization activity of Ti-MWW-4.

Based on the characterization results from XRD and N_2 physisorption, the framework structure of MWW appears well preserved after acid treatment and incorporation of Ti. According to the results from the FT-IR and XPS analysis, the majority of Ti species were successfully incorporated into the MWW framework. Therefore, Ti-MWW has a certain number of active sites due to the introduction of titanium. It can be expected that the prepared Ti-MWW sample is a potential catalyst for the desulfurization reaction.

2. Effects of Ti Incorporation on DBT Conversion

To examine the effects of Ti incorporation in the MWW samples on the DBT conversion performance, CM-MWW, AT-MWW, and Ti-MWW with different Ti content were tested for DBT con-

version under the same reaction conditions and these results are shown in Fig. 6(a). At 50 min of reaction, the conversion rates of DBT were 18.5% and 22.4%, respectively, for CM-MWW and AT-MWW. This shows that both CM-MWW and AT-MWW have very poor catalytic activity for the DBT conversion. When Ti was introduced into MWW, the catalytic activities were significantly enhanced. Within 10 min of starting the reaction, the conversion rate increased rapidly for Ti-MWW-1, -2, -3, and -4, reaching 58.4,

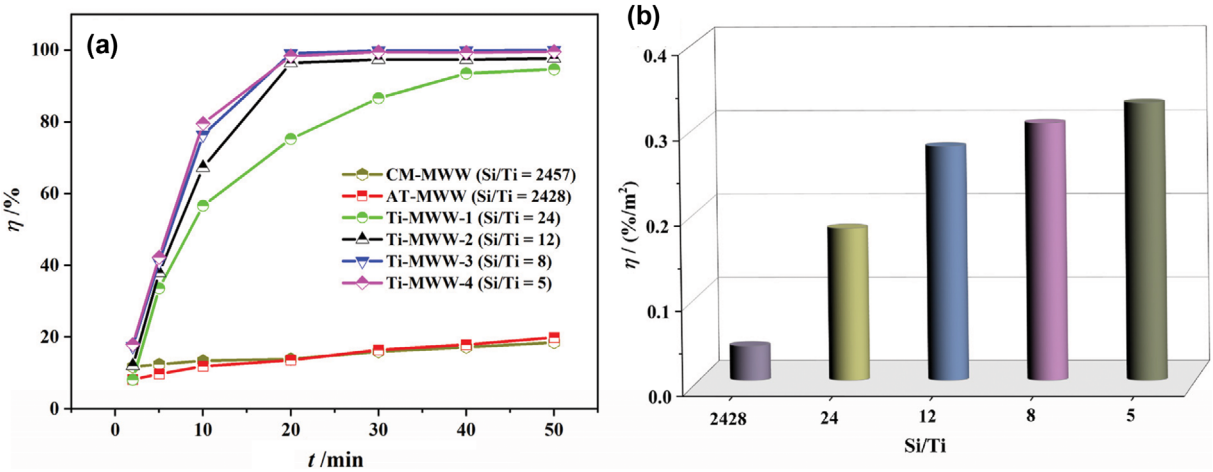

Fig. 6. (a) Dependence of the DBT conversion versus reaction time on the incorporation amount of Ti in MWW catalysts and (b) comparison of the surface-area-normalized DBT conversion at 10 min of the reaction. Reaction condition: m (cat.)=10 mg, O/S=3 : 1, V (model oil)=10 mL, T=70 °C, and v=750 rpm.

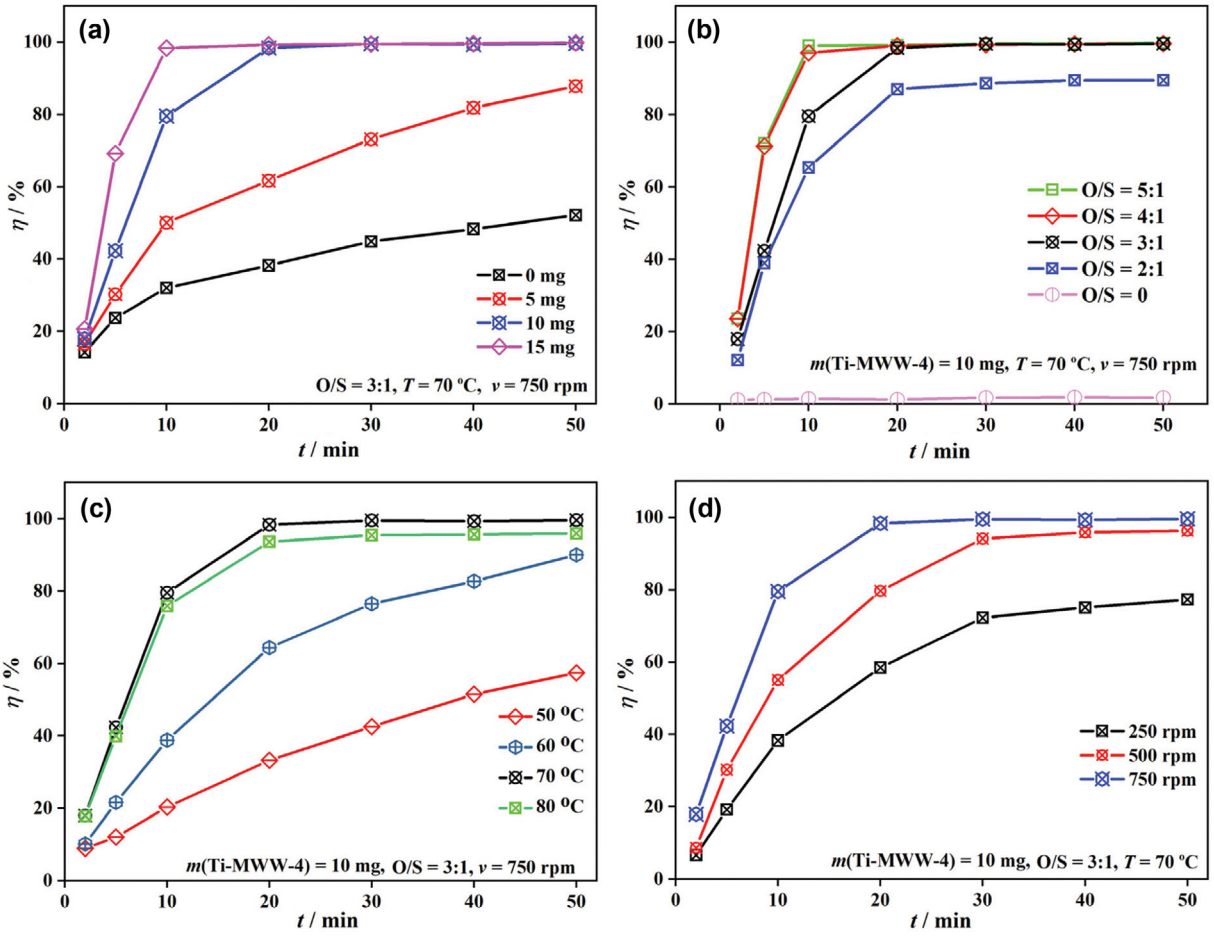

Fig. 7. Reaction parameters for DBT conversion (a) the amount of Ti-MWW-4, (b) the O/S, (c) the reaction temperature, and (d) the stirring speed. Other experimental conditions: V (model oil)=10 mL and t=50 min.

88.3, 94.4, and 99.0%, respectively. When the reaction went from 10 to 50 min, the conversion rates increased slowly.

As shown in Fig. 6(b), the specific activity (the conversion rate normalized by the surface area) of Ti-MWW-1, -2, -3, and -4 was 4.4, 6.8, 7.4, and 8.0 times of AT-MWW, respectively, at 10 min of the reaction time. It is clear that as the molar ratio of Si to Ti (Si/Ti) decreases (the content of Ti increases), the DBT conversion gradually increases. When the content of Si/Ti reached 8 (Ti-MWW-3) or 5 (Ti-MWW-4), the DBT conversion increased slightly. This indicates that the catalytic activity would reach a certain upper limit with the increase of the Ti content.

3. Effects of Different Reaction Conditions on DBT Conversion

Fig. 7(a) shows the effect of the amount of Ti-MWW-4 on DBT conversion. In the absence of a catalyst, the conversion of DBT increased slowly as the reaction proceeded. This indicates that CHP can react slowly with DBT at 70 °C. With the addition of Ti-MWW-4, the DBT conversion increases rapidly. When the amount of Ti-MWW-4 was 5 mg and 10 mg, the DBT conversion reached 87.8% and 99.6%, respectively. There was no significant increase when the amount of Ti-MWW-4 was increased to 15 mg. Therefore, 10 mg of Ti-MWW-4 seems to be close to the optimum catalyst dosage.

Fig. 7(b) shows the effect of the amount of CHP on the DBT conversion. In the absence of CHP, the conversion (reduction) of DBT was about 1.8%. Strictly speaking, this decrease in the amount of DBT is due to the adsorption on Ti-MWW-4. With the addition of CHP, the DBT conversion increased rapidly. The DBT conversion exceeded 99% within 50 min at O/S≥3 : 1. Since the excess oxidant further contaminated the quality of the oil and also caused safety issues, an O/S ratio of 3:1 was adopted.

As shown in Fig. 7(c), the DBT conversion at 50, 60, 70, and 80 °C was found to be 57.4, 90.0, 99.6, and 98.9%, respectively after 50 min of reaction. These results show that the best DBT conversion was obtained at 70 °C. However, at higher temperatures above 70 °C, the DBT conversion reduced slightly. This can probably be attributed to the rapid decomposition of CHP at higher temperature. Using too high of a temperature would lead to a slight decrease in the oxidation rate of DBT, and this was also observed in the case of using H_2O_2 [33] and O_2 [46] as oxidants. Considering the higher energy consumption and unfavorable DBT conversion at high temperature, a near optimal reaction temperature was set to 70 °C.

Stirring speed is also an important external driving force in the reaction process in current solid-liquid reaction systems [47,48]. As shown in Fig. 7(d), when the stirring speed was set to 250, 500, and 750 rpm, the corresponding DBT conversion was 77.3, 96.3, and 99.6%, respectively. This is due to the higher stirring speed being beneficial to the increasing the full contact of the catalyst, DBT, and CHP. Therefore, 750 rpm was chosen as the near optimal stirring speed for the reaction systems of interest.

4. Catalytic Oxidation Kinetics of DBT

Some previous studies have reported that the oxidation kinetics of DBT obey the pseudo-first-order rule [21,49]. This is based on the assumption that the oxidant is present in a greatly excessive amount and the concentration of the oxidant is thus treated as a constant. A more detailed description is given in Eqs. (S1)-(S3) in SI. Here, the plots of $\ln(1-\eta)$ versus reaction time were preferentially fitted to straight lines at different temperatures as shown in Fig. 8(a). These results indicate that the kinetic curves are well treated by the pseudo-first-order rate equation at reaction temperatures of 50 °C and 60 °C with the square of the correlation coefficients (R^2) both above 0.99. However, the fitted curves showed poor linear correlation at 70 °C and 80 °C with R^2 both below 0.86. This may be because the CHP concentration cannot be regarded as a constant in the kinetics equations when the reaction temperature exceeds 70 °C.

To consider the effect of the CHP concentration, the rate equation of a pseudo-1.5-order reaction was further tried to fit the kinetics data (Eqs. (S4) and (S5) in SI). As depicted in Fig. 8(b), the plots of $(1-\eta)^{-0.5}$ versus reaction time were fitted to the straight lines at different temperatures. The R^2 at 70 °C and 80 °C was increased to 0.9594 and 0.8468, respectively. The linear correlation of the fitting curve was still unsatisfactory at 80 °C, which may be due to the strong decomposition of CHP itself at such a high temperature. Moreover, the kinetic curves had a good linear relationship at 50 °C and 60 °C. Therefore, it is more reasonable to attribute the oxidation reaction of DBT to pseudo-1.5-order reaction from

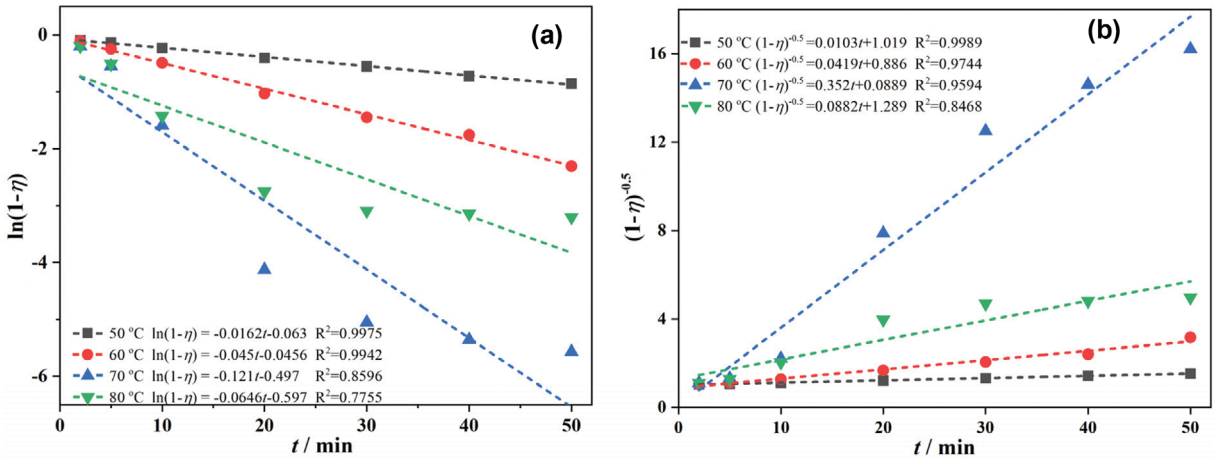

Fig. 8. (a) Plots of $\ln(1-\eta)$ versus reaction time and (b) $(1-\eta)^{-0.5}$ versus reaction time at different temperature.

50 to 70 °C. This is very interestingly different from the first-order kinetics previously observed in most one-step oxidative-adsorptive processes [50]. Therefore, the adsorbent and the oxidant simultaneously affect the catalytic oxidation kinetics of DBT. It is also different from the second-order kinetics observed in stepwise oxidation and stepwise adsorption. According to the slope (k_2) of the fitted rate equation (Fig. 8(b)), the rate constant (k) at 50, 60, and 70 °C was 0.737, 0.237, and 1.993 $mol^{-0.5} \cdot L^{0.5} \cdot min^{-1}$, respectively. The apparent activation energy was estimated to be about 151.3 kJ·mol^{-1} by the Arrhenius equation.

5. Comparison of DBT Conversion over Ti-containing Zeolites

To make a comprehensive comparison, the catalytic performance of several representative Ti-containing zeolites for DBT conversion is listed in Table 3. For DBT conversion, the conventional TS-1 had almost no activity due to the limitation of its pore size [51]. The number of turnover frequencies (TOF) was significantly increased in the improved TS-1 system that has a relatively large pore size such as for mesoporous TS-1 (Meso-TS-1) [52,53] and hierarchical TS-1 (HTS-1) [54,55]. It needs to be noted that HTS-1b exhibited the highest TOF number among these catalysts [56]. The TOF number reached 114.9 h^{-1}. Higher catalytic performance was also observed for DBT conversion in other mesoporous Ti-containing zeolites. The TOF number over Ti-SBA-2 [35] or Ti-containing hierarchical Beta (Ti-B-M-DA) [42] was 48.8 h^{-1} or 58.8 h^{-1}, respectively. Furthermore, the higher TOF numbers may also be attributed to the use of the oil soluble oxidant TBHP. Obviously, for some mesoporous Ti-containing zeolites such as, Ti-MCM-41 [51], Ti-MM-05 [32], Ti-Beta [57], Ti-HMS [58,59], and Ti-containing wormlike mesoporous silica (Ti-WMS) [60] their TOF numbers were found to be no more than 5 when H_2O_2 was used as oxidant in these systems. Due to the immiscibility of H_2O_2 and oil, extractants such as water, methanol, and acetonitrile, were usually introduced into ODS to accelerate the reaction. Theoretical studies showed that the extractant can combine with the Ti active center to form a complex, which may occupy some active sites [61]. As shown in Table 3, the TOF numbers of the ODS without extractant were generally higher than those with the extractant, which is consistent with the previous mentioned theoretical analysis.

Here, the TOF numbers over Ti-MWW were calculated according to the conversion rate at 10 min. Three different oxidants--H_2O_2, TBHP, and CHP--were tested. These results show that the hydrophilic H_2O_2 could barely oxidize DBT over Ti-MWW, while the lipophilic TBHP and CHP show higher TOF numbers. The TOF numbers for TBHP and CHP were 25.4 h^{-1} and 40.1 h^{-1}, respectively, which were significantly higher than that previously reported 2.3 h^{-1} over Ti-MWW/H_2O_2 [62]. Consequently, these results show that Ti-MWW/CHP is a potential high activity desulfurization ODS system.

Table 3. Comparison of catalytic performance over some respective Ti-containing zeolites towards DBT conversion in ODS

No.	Catalyst	Ti content /wt%	Model oil	Initial sulfur content/ppm[b]	Oxidant	O/S	Extractant	Temperature/ °C	TOF/h^{-1}	Refs.
1	TS-1	1.8[a]	DBT in *n*-octane	240	H_2O_2	4 : 1	Methanol	60	0	[51]
2	Meso-TS-1	0.98[a]	DBT in *n*-octane	1,000	H_2O_2	2 : 1	Water	60	3.7	[52]
3	Meso-TS-1	0.89[a]	DBT in *n*-heptane	200	TBHP	15 : 1	None	80	32.2	[53]
4	HTS-1	2.3[a]	DBT in *n*-octane	500	TBHP	2 : 1	None	60	15	[54]
5	HTS-1	2.5[a]	DBT in *n*-octane	1,000	TBHP	3 : 1	None	60	8.8	[31]
6	HTS-1	2.5[a]	DBT in *n*-octane	500	TBHP	2 : 1	None	60	8.9	[55]
7	HTS-1b	2.02	DBT in *n*-octane	1,000	TBHP	4 : 1	None	60	114.9	[56]
8	Ti-MCM-41	1.8[a]	DBT in *n*-octane	240	H_2O_2	4 : 1	Methanol	60	0.7	[51]
9	Ti-MM-0.5	3.58	DBT in *n*-octane	1,000	H_2O_2	6 : 1	Acetonitrile	60	4.3	[32]
10	Ti-SBA-2	5.5	DBT in *n*-decalin	500	TBHP	3 : 1	None	60	48.8	[35]
11	Ti-Beta	0.63[a]	DBT in acetonitrile	584	H_2O_2	2.4 : 1	None	60	5	[57]
12	Ti-B-M-DA	5.5	DBT in *n*-octane	1,000	TBHP	6 : 1	None	60	58.8	[42]
13	Ti-HMS	5.3[a]	DBT in *n*-decane	500	CYHPO	2 : 1	None	60	0.93	[19]
14	Ti-HMS	0.88[a]	DBT in acetonitrile	584	H_2O_2	2.4 : 1	None	60	1.8	[57]
15	Ti-HMS	4.1[a]	DBT in *n*-octane	500	H_2O_2	40 : 1	None	60	0.6	[58]
16	Ti-HMS/TS-1	1.5[a]	DBT in *n*-octane	182	H_2O_2	4 : 1	Methanol	60	1.82	[59]
17	Ti-WMS	1.5[a]	DBT in *n*-octane	182	H_2O_2	4 : 1	Methanol	60	0.61	[60]
18	Ti-MWW	2.2[a]	DBT in isooctane	1,000	H_2O_2	4 : 1	Acetonitrile	70	2.3	[62]
19	Ti-MWW	11.1	DBT in *n*-decane	500	H_2O_2	3 : 1	None	70	0.03[c]	This work
20	Ti-MWW	11.1	DBT in *n*-decane	500	TBHP	3 : 1	None	70	25.4[c]	This work
21	Ti-MWW	11.1	DBT in *n*-decane	500	CHP	3 : 1	None	70	40.1[c]	This work

[a]Ti content was calculated according to Si/Ti ratio.

[b]Some literatures use the unit of mg/L (ppmv), the others use unit of mg/kg or μg/g (ppmw), but the volume (mL) or mass (mg) unit was used to measure the corresponding quantity of model oil. Therefore, the unit here was uniformly marked as ppm, which does not affect the calculation of sulfur quantity.

[c]Reaction condition: m (Ti-MWW-4)=10 mg, O/S=3 : 1, V (model oil)=10 mL, T=70 °C, t=10 min, and v=750 rpm.

6. Effects of Olefins and Aromatics on DBT Conversion

In addition to alkanes, olefins and aromatics are essential components of real fuel oils. Therefore, we further investigated the effects of the presence of olefins and aromatics on DBT conversion in the current reactions investigated in this report. Here, 1-octene, 1,5-cyclooctadiene, 1,2,3,4-tetrahydronaphthalene, and naphthalene were, respectively, selected as examples of monoolefins, diolefins, monocyclic aromatic hydrocarbons and bicyclic aromatic hydrocarbons to examine their effects on DBT conversion. As shown in Fig. 9, the amount of olefins and aromatics added ranged from 1

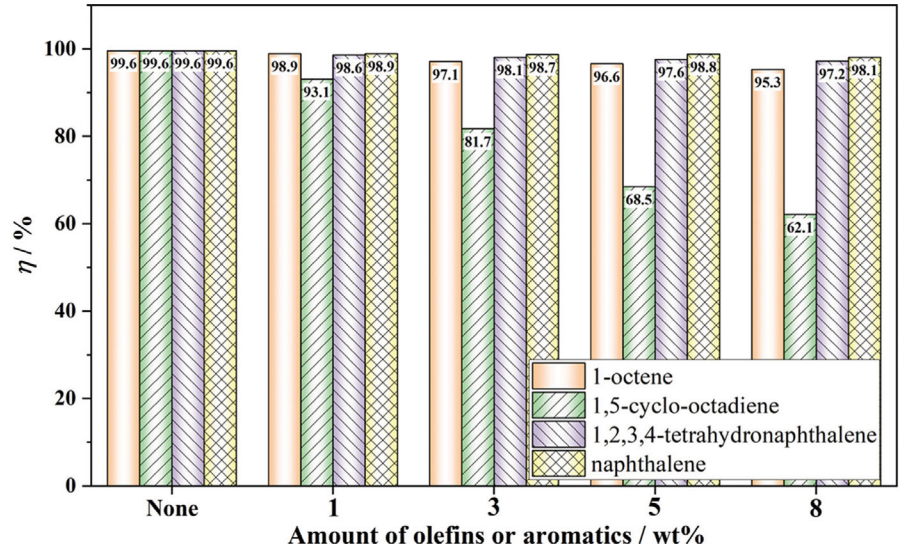

Fig. 9. Effects on the DBT conversion of the amount of olefins or aromatics. Experimental conditions: T=70 °C, V (model oil)=10 mL, m (Ti-MWW-4)=10 mg, O/S=3 : 1, v=750 rpm, and t=50 min.

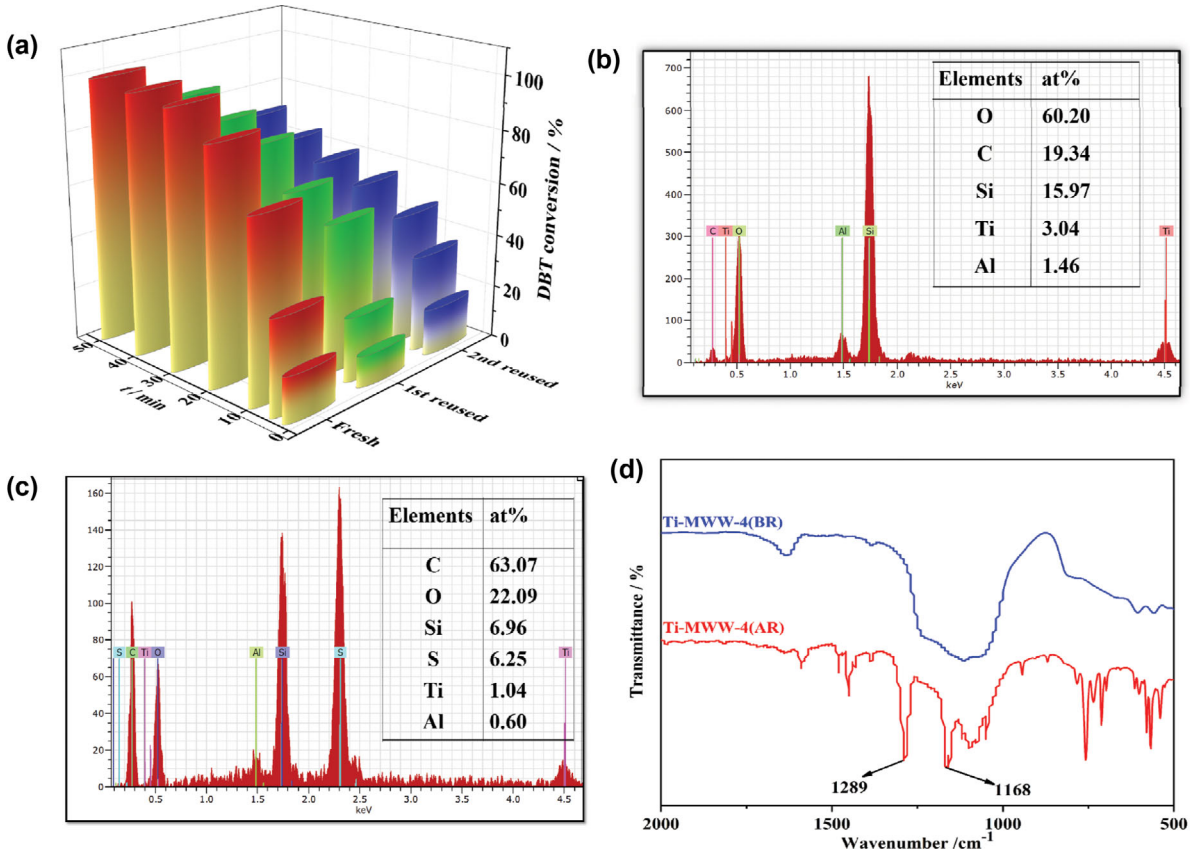

Fig. 10. (a) DBT conversion under Ti-MWW-4 recycling, experimental conditions see Fig. 6; EDS test of Ti-MWW-4: (b) before reaction and (c) after reaction; (d) FT-IR spectra of Ti-MWW-4.

to 8 wt% to be tested, respectively. When 1-octene, 1,5-cyclooctadiene, 1,2,3,4-tetrahydronaphthalene, and naphthalene were added at 8 wt%, the DBT conversion decreased to 95.3, 62.1, 97.2, and 98.1%, respectively. Hence, it was obvious that the order of inhibition of DBT conversion by different olefins and aromatic was as follows: 1,5-cyclo-octadiene>1-octene>1,2,3,4-tetrahydronaphthalene> naphthalene, which suggests that the aromatics have a weaker inhibition of DBT conversion than olefins in the current reaction systems examined. This is because aromatic hydrocarbons are relatively stable. Meanwhile, the DBT conversion decreased significantly with the increase of the 1,5-cyclooctadiene concentration. This indicates that the diolefin inhibited significantly the DBT conversion because the diolefin was more susceptible to oxidation.

7. Evaluation of Catalyst Stability

The stability of the Ti-MWW-4 systems was investigated by reusing the original catalyst continuously. The upper oil phase was collected by static layering (at the end of each DBT conversion test) and then 10 mL of fresh model oil and the corresponding certain amount of CHP were added. Fig. 10(a) depicts the decrease in the activity of Ti-MWW-4 after three uses. When used for the second time, the DBT conversion was reduced to 70.1% compared to 99.6% for the fresh samples. The rapid decrease of the Ti-MWW-4 activity may be attributed to the occupation of its surface-active sites. Therefore, it is necessary to investigate the changes of the surface elements of Ti-MWW-4 after reuse.

EDS is a powerful tool for identifying the changes of the elements on the surface of catalysts. As shown in Fig. 10(b), the sample before reaction (BR) clearly contains C, O, Al, Ti, and Si elements. The C element may be from contamination during the test (adsorbed CO_2 or carbon-containing tape used in the sample preparation). As shown in Fig. 10(c), the sample after reaction (AR) clearly contains C, O, Al, Ti, Si, and S elements. Among them, the S element was attributed to DBT or the oxidation product(s) of DBT adsorbed by the catalyst. Although EDS does not accurately quantify the elemental content of the catalyst due to its inherent resolution accuracy, it can be roughly used to compare changes in the content of each element. It is apparent that the S element is not detected in the fresh Ti-MWW-4 (BR) and its atomic percentage (at%) reaches 6.25% after reaction. Meanwhile, the C element gained from 19.34 (BR) to 63.07 at% (AR). This clearly indicates that the S-containing compounds were adsorbed on the surface of the Ti-MWW-4.

FT-IR was further used to confirm the changes of the functional groups contained in the catalyst after the reaction. FT-IR spectra (2,000-500 cm^{-1}) of Ti-MWW-4 before and after the AODS reaction occurred are shown in Fig. 10(d). The strong intensity peaks at 1,289 cm^{-1} and 1,168 cm^{-1} were attributed to asymmetric and symmetric stretching of the -SO_2- functional group present in the DBT-sulfone ($DBTO_2$), respectively. These results demonstrate that Ti-MWW-4 and CHP oxidize DBT to $DBTO_2$, which was then adsorbed by Ti-MWW-4. This phenomenon further illustrates that the current reaction was a reaction-adsorption combined desulfurization process. In addition, no characteristic peak (strong absorption at 1,060-1,020 cm^{-1}) of DBT-sulfoxide (DBTO) was observed. This result indicates that the formation of the DBT-sulfoxide or elimination from the surface of the active site is a rate determining step.

8. Evaluation of Catalyst Regenerability

The used Ti-MWW-4 was regenerated by calcination to remove the organic residues on the surface. The DBT conversion of the regenerated Ti-MWW-4 obtained by calcination at 450, 500, 550, and 600 °C in air for 12 h is shown in Fig. 11(a). The DBT conversion of Ti-MWW-4 regenerated at 500, 550 and 600 °C was 98.0%, 98.6%, and 96.4%, respectively, showing Ti-MWW-4 recovered a comparable catalytic activity after calcination. The DBT conversion of Ti-MWW-4 regenerated at 600 °C decreased slightly, which was due to the collapse of Ti-MWW pores caused by too high calcination temperature. It was also observed that DBT conversion of Ti-MWW-4 regenerated at 450 °C was only 82.5%. This is because the organic residues on the catalyst surface were not completely removed at a lower calcination temperature.

Fig. 11(b) shows the XRD patterns of the fresh, used, and regenerated samples. The disappearance of most of the crystal peaks in the used sample can be attributed to the adsorption of oxidized sulfur-containing compounds on the surface, indicating that the catalyst might have been less active. However, calcination was able

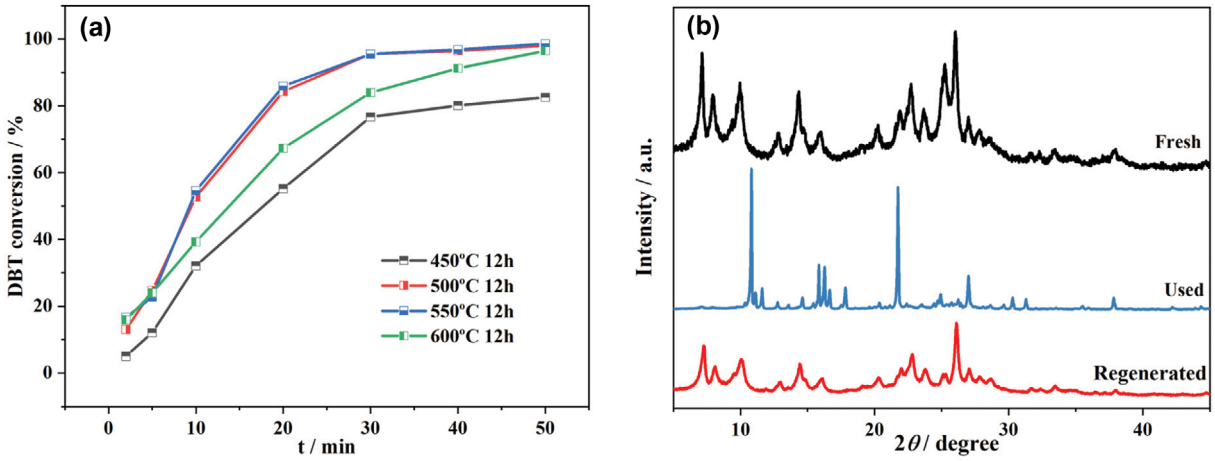

Fig. 11. (a) DBT conversion of the regenerated Ti-MWW-4 at different calcination temperatures, and (b) XRD patterns for the Ti-MWW-4 samples.

to restore its catalytic performance as stated in the Fig. 7(a) and Fig. 7(b) results; it is obvious that these phases will be present on the XRD pattern of the calcined sample. This is due to the decomposition of most of the sulfur-containing organics adsorbed on the catalyst surface at high temperature.

9. Probable Reaction Mechanism

The GC spectra of oil samples with different reaction times clearly reflect the changes of the oil phase components, as shown in Fig. 12(a). The relative intensities of the peaks of *n*-decane and *n*-tetradecane (internal standard) remained unchanged in this process, which indicates that they were not involved in the CHP oxidation. As the reaction progressed, the peak intensities of CHP and DBT gradually weakened. The peak for DBT disappeared almost completely after 30 min of reaction. Meanwhile, the peaks of the reduction product (CA) of CHP and the oxidation products (DBTO and $DBTO_2$) of DBT gradually appeared. Because DBTO was unstable, it was finally converted to $DBTO_2$ when the reaction reached 50 min. The mass spectra (Fig. 12(b)) further confirmed that the obtained products were CA and $DBTO_2$. When the reaction time increased from 10 to 50 min, the intensity of $DBTO_2$ peak did not increase obviously, which indicates that $DBTO_2$ was only slightly soluble in the oil phase. The content of the dissolved $DBTO_2$ in the oil phase was ~10% of that of $DBTO_2$ calculated based on the total DBT content. The rest of the $DBTO_2$ will be separated from the oil phase and adsorbed on the Ti-MWW surface. The EDS test, mentioned above, demonstrated that there are S and C elements on the Ti-MWW surface after reaction. Note that residual $DBTO_2$ and CHP are still oil pollutants, which can be further removed by adding other separation processes in actual production on a larger scale. However, this is beyond the scope of this work and only a simple refining process is proposed in Fig. S2 in SI.

The proposed stepwise reaction mechanism is shown in Scheme 1. In the first step, the defective Ti-OH species are oxidized by CHP to possible Ti-hydroperoxo intermediates and CHP is reduced

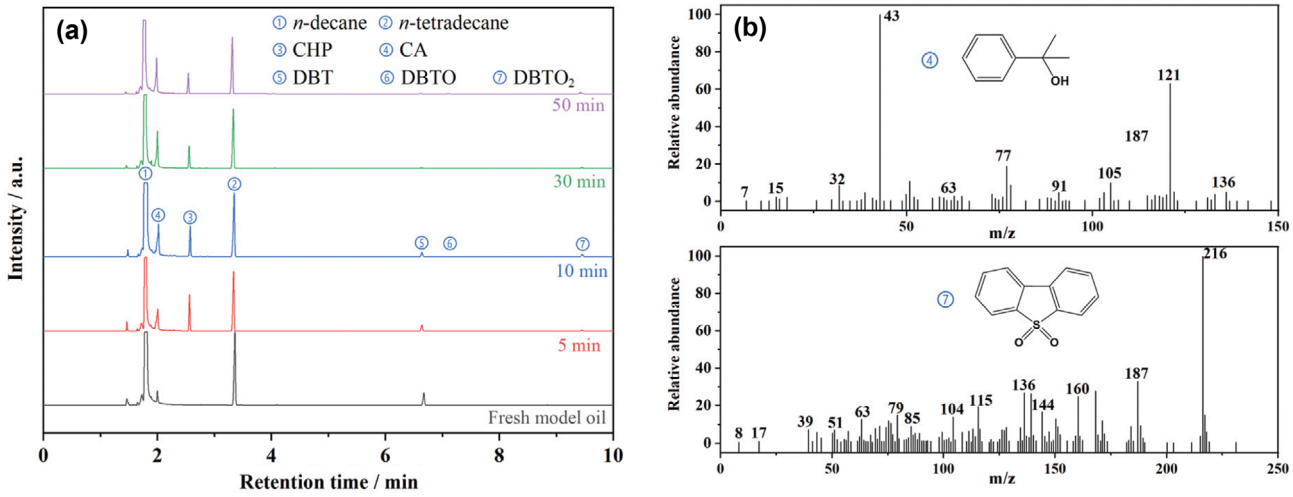

Fig. 12. (a) GC spectra of oil samples with different reaction time, (b) MS spectra of CA and $DBTO_2$.

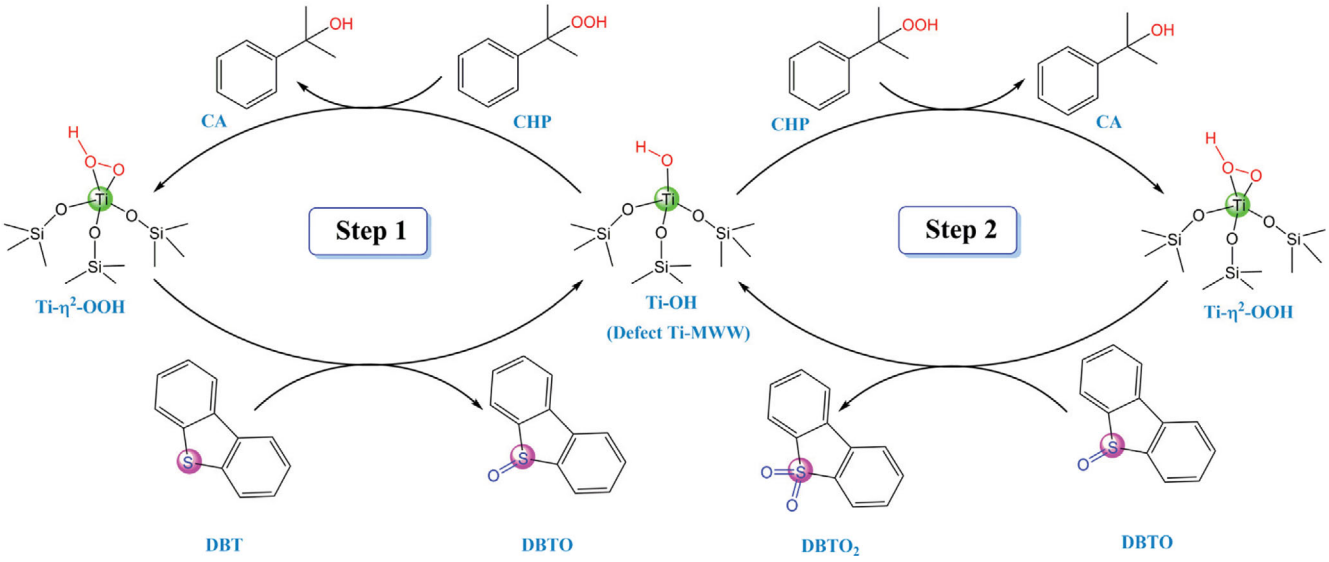

Scheme 1. Proposed reaction mechanism of DBT by CHP and Ti-MWW.

to CA. Among the formed Ti-hydroperoxo intermediates, the bidentate Ti-η^2-OOH is a relatively stable active intermediate, which was inferred from results of previous experiments and theoretical studies of the Ti-MWW/H_2O_2 system [61]. Then Ti-η^2-OOH reacts with DBT to form DBTO. In the second step, DBTO and Ti-η^2-OOH further form the final product $DBTO_2$, which completes the oxidation process.

CONCLUSIONS

A series of Ti-MWW with different Ti content were successfully prepared by using MWW as a raw material through acid treatment and calcination with titanocene dichloride. The Ti-MWW was successfully applied as a catalyst and as an adsorbent in the desulfurization tests of a model oil containing DBT and employing CHP as the oxidant. The DBT conversion reached 99.6% and the TOF number was 40.1 h^{-1} under the conditions with a catalyst of 0.01 g, a model oil of 10 mL, a temperature of 70 °C, and an O/S ratio of 3 : 1. The results showed that Ti-MWW/CHP is a potential high activity desulfurization AODS system. The kinetics analysis revealed that the oxidation kinetics of DBT in the Ti-MWW/CHP system accorded with a pseudo-1.5-order rule. A proposed reaction mechanism showed that DBT converted to $DBTO_2$ through a two-step reaction with the assistance of the active intermediate Ti-η^2-OOH. The order of inhibition of the DBT conversion for selected oil compositions was 1,5-cyclo-octadiene>1-octene> 1,2,3,4-tetrahydronaphthalene>naphthalene. The spent Ti-MWW can easily restore its catalytic activity by calcination. This study will inspire the exploration of similar AODS systems using abundant and available zeolite catalysts and oil solvent oxidants for utilization in clean fuel production technology.

ACKNOWLEDGEMENTS

Authors gratefully acknowledge Natural Science Foundation of Guangdong Basic and Applied Basic Research Fund (2021A15150 10278), the Training Program for Guangdong Provincial Characteristic Innovation Projects of Universities (2018KTSCX149), Projects of PhDs' Start-up Research of Guangdong University of Petrochemical Technology (2020bs002), Open Fund of Guangdong Provincial Key Laboratory of Petrochemical Pollution Process and Control, Guangdong University of Petrochemical Technology (No. 2018B030322017), Petroleum Technology Development Fund (PTDF), Nigeria.

SUPPORTING INFORMATION

Additional information as noted in the text. This information is available via the Internet at http://www.springer.com/chemistry/journal/11814.

REFERENCES

1. L. Zhang, Z. Chen, S. Zheng, G. Cai, W. Fu, T. Tang and M. He, *Ind. Eng. Chem. Res.*, **59**, 12338 (2020).
2. Y. S. Al-Degs, A. H. El-Sheikh, R. Z. Al Bakain, A. P. Newman and M. A. Al-Ghouti, *Energy Technol.*, **4**, 679 (2016).
3. J. J. Raj, S. Magaret, M. Pranesh, K. C. Lethesh, W. C. Devi and M. I. A. Mutalib, *J. Clean. Prod.*, **213**, 989 (2019).
4. Y. Song, D. Yang, S. Yu, X. Teng, Z. Chang, F. Pan, X. Bu, Z. Jiang, B. Wang, S. Wang and X. Cao, *Sep. Purif. Techol.*, **210**, 258 (2019).
5. T. Geng, J. He, L. Hu and J. Li, *Inorg. Chem. Commun.*, **101**, 103 (2019).
6. J. Wen, D. Zhao, Y. Lu, J. Huang, Y. Li, H. Zhang and A. Li, *Korean J. Chem. Eng.*, **36**, 1131 (2019).
7. M. Gan, G. Yang, Z. Wang, X. Sui and Y. Hou, *Energy Fuel*, **34**, 778 (2020).
8. L. P. Rivoira, B. C. Ledesma, J. M. Juárez and A. R. Beltramone, *Fuel*, **226**, 498 (2018).
9. M. Dana, S. Shahhosseini, M. A. Sobati, A. R. Ansari and M. Asadollahzadeh, *Energy Fuel*, **34**, 1041 (2020).
10. D. Yue, J. Lei, Y. Peng, J. Li and X. Du, *Fuel*, **226**, 148 (2018).
11. M. Rogosic, A. Sander, V. Kojic and J. P. Vukovic, *Fluid Phase Equilibr.*, **412**, 39 (2016).
12. J. F. Palomeque-Santiago, R. López-Medina, R. Oviedo-Roa, J. Navarrete-Bolaños, R. Mora-Vallejo, J. A. Montoya-de la Fuente and J. M. Martínez-Magadán, *Appl. Catal. B: Environ.*, **236**, 323 (2018).
13. M. A. Rezvani, M. Shaterian, F. Akbarzadeh and S. Khandan, *Chem. Eng. J.*, **333**, 537 (2018).
14. D. Yue, J. Lei, L. Zhou, Z. Guo, X. Du and J. Li, *Catal. Lett.*, **148**, 1100 (2018).
15. A. Bazyari, A. A. Khodadadi, A. H. Mamaghani, J. Beheshtian, L. T. Thompson and Y. Mortazavi, *Appl. Catal. B Environ.*, **180**, 65 (2016).
16. Q. Zhou, S. Fu, M. Zou, Y. He, Y. Wu and T. Wu, *RSC Adv.*, **5**, 69388 (2015).
17. W. N. W. Abdullah, W. A. W. Abu Bakar, R. Ali and Z. Embong, *Clean Technol. Environ.*, **17**, 433 (2015).
18. C. Yang, K. Zhao, Y. Cheng, G. Zeng, M. Zhang, J. Shao and L. Lu, *Sep. Purif. Techol.*, **163**, 153 (2016).
19. X. Lin, X. Zeng, R. Zhou and H. Wang, *React. Kinet. Mech. Cat.*, **126**, 353 (2019).
20. C. Shen, Y. J. Wang, J. H. Xu and G. S. Luo, *Chem. Eng. J.*, **259**, 552 (2015).
21. Y. Chen, H. y. Song, Y. Z. Lu, H. Meng, C. X. Li, Z. G. Lei and B. H. Chen, *Ind. Eng. Chem. Res.*, **55**, 10394 (2016).
22. V. A. Ostroumova and A. L. Maksimov, *Petrol. Chem.*, **59**, 788 (2019).
23. J. Grzybek, W. J. Roth, B. Gil, A. Korzeniowska, M. Mazur, J. Cejka and R. E. Morris, *J. Mater. Chem. A*, **7**, 7701 (2019).
24. Y. Zhang, M. Kubu, M. Mazur and J. Cejka, *Catal. Today*, **324**, 135 (2019).
25. H. Wang, I. Jibrin and X. Zeng, *Front. Chem. Sci. Eng.*, **14**, 546 (2020).
26. J. Yin, H. Xu, B. Wang, W. Tian, J. Yin, J. Jiang and P. Wu, *Catal. Sci. Technol.*, **10**, 6050 (2020).
27. A. Gawarecka and A. Wroblewska, *React. Kinet. Mech. Cat.*, **124**, 523 (2018).
28. M. Zhu, Y. Liu, Y. Yao, J. Jiang, F. Zhang, Z. Yang, Z. Lu, I. Kumakiri, X. Chen and H. Kita, *Micropor. Mesopor. Mater.*, **268**, 84 (2018).
29. H. Wang, M. Yu and Z. Lin, *J. Mol. Model.*, **25**, 106 (2019).
30. S. Du, X. Chen, Q. Sun, N. Wang, M. Jia, V. Valtchev and J. Yu,

Chem. Commun., **52**, 3580 (2016).
31. Q. Du, Y. Guo, H. Duan, H. Li, Y. Chen and H. Liu, *Fuel*, **188**, 232 (2017).
32. K. Leng, Y. Sun, X. Zhang, M. Yu and W. Xu, *Fuel*, **174**, 9 (2016).
33. U. Arellano, J. A. Wang, L. F. Chen, G. Z. Cao, M. Asomoza and S. Cipagauta, *J. Mol. Catal. A: Chem.*, **421**, 66 (2016).
34. F. Wang, G. Wang, L. Bing, Y. Wang, A. Tian and K. Yi, *Int. J. Chem. React. Eng.*, **16**, 20170112 (2018).
35. C. Shi, W. Wang, N. Liu, X. Xu, D. Wang, M. Zhang, P. Sun and T. Chen, *Chem. Commun.*, **51**, 11500 (2015).
36. B. Tang, W. Dai, X. Sun, N. Guan, L. Li and M. Hunger, *Green Chem.*, **16**, 2281 (2014).
37. M. Yan, F. Jin, Y. Ding, G. Wu, R. Chen, L. Wang and Y. Yan, *Ind. Eng. Chem. Res.*, **58**, 4764 (2019).
38. P. Lu, L. Gomez-Hortiguela and M. A. Camblor, *Chem-Eur. J.*, **25**, 1561 (2019).
39. B. Li, N. Wu, K. Wu, J. Liu, C. Han and X. Li, *RSC Adv.*, **5**, 16598 (2015).
40. L. Wu, X. Deng, S. Zhao, H. Yin, Z. Zhuo, X. Fang, Y. Liu and M. He, *Chem. Commun.*, **52**, 8679 (2016).
41. J. Wang, F. Zhang, W. Hua, Y. Yue and Z. Gao, *Catal. Commun.*, **18**, 63 (2012).
42. K. Leng, X. Li, G. Ye, Y. Du, Y. Sun and W. Xu, *Catal. Sci. Technol.*, **6**, 7615 (2016).
43. A. Bazyari, A. A. Khodadadi, A. H. Mamaghani, J. Beheshtian, L. T. Thompson and Y. Mortazavi, *Appl. Catal. B: Environ.*, **180**, 65 (2016).
44. B. Tang, W. Dai, X. Sun, N. Guan, L. Li and M. Hunger, *Green Chem.*, **16**, 2281 (2014).
45. Q. Du, Y. Guo, P. Wu, H. Liu and Y. Chen, *Micropor. Mesopor. Mater.*, **275**, 61 (2019).
46. Y. Gao, Z. Lv, R. Gao, G. Zhang, Y. Zheng and J. Zhao, *J. Hazard. Mater.*, **359**, 258 (2018).
47. Z. Li, Y. Cui, C. Li and Y. Shen, *Sep. Purif. Techol.*, **219**, 9 (2019).
48. L. Li, J. Zhang, C. Shen, Y. Wang and G. Luo, *Fuel*, **167**, 9 (2016).
49. C. Shen, Y. J. Wang, J. H. Xu and G. S. Luo, *Chem. Eng. J.*, **259**, 552 (2015).
50. M. D. G. d. Luna, M. L. Samaniego, D. C. Ong, M.-W. Wan and M.-C. Lu, *J. Clean. Prod.*, **178**, 468 (2018).
51. Q. Lv, G. Li and H. Sun, *Fuel*, **130**, 70 (2014).
52. Y. Fang and H. Hu, *Catal. Commun.*, **8**, 817 (2007).
53. S. T. Yang, K. E. Jeong, S. Y. Jeong and W. S. Ahn, *Mater. Res. Bull.*, **47**, 4398 (2012).
54. S. Du, F. Li, Q. Sun, N. Wang, M. Jia and J. Yu, *Chem. Commun.*, **52**, 3368 (2016).
55. S. Du, Q. Sun, N. Wang, X. Chen, M. Jia and J. Yu, *J. Mater. Chem. A*, **5**, 7992 (2017).
56. Q. Du, Y. Guo, P. Wu and H. Liu, *Micropor. Mesopor. Mater.*, **264**, 272 (2018).
57. V. Hulea, F. Fajula and J. Bousquet, *J. Catal.*, **198**, 179 (2001).
58. S. Cui, F. Ma and Y. Wang, *React. Kinet. Cat. Let.*, **92**, 155 (2007).
59. C. Jin, G. Li, X. Wang, Y. Wang, L. Zhao and D. Sun, *Micropor. Mesopor. Mater.*, **111**, 236 (2008).
60. C. Jin, G. Li, X. Wang, L. Zhao, Y. Wang and D. Sun, *Top. Catal.*, **49**, 118 (2008).
61. H. Bian, H. Zhang, D. Li, Z. Duan, H. Zhang, S. Zhang and B. Xu, *Micropor. Mesopor. Mater.*, **294**, 109837 (2020).
62. S. Cheng, Y. Liu, J. Gao, L. Wang, X. Liu, G. Gao, P. Wu and M. He, *Chin. J. Catal.*, **27**, 547 (2006).